Cambridge Journal for Junior Scientists
Volume 2, Number 2, 213–252, 2025

Ups and downs of objects in supersaturated fluid: the dynamics of open gas-solid coupled systems*

Haiyi Luo and Yunyi Yang

When a body is submerged in a supersaturated fluid, a layer of bubbles may form on its surface, causing the body to ascend. As these bubbles get cleaned off at the fluid-air interface, the object will sink once more, creating a cyclical "dancing" motion under conditions of sufficient supersaturation. This fascinating phenomenon, observed across various systems, has garnered significant research attention. Previous studies have concentrated on the theory of bubble nucleation and evolution, as well as simulations of object movement within supersaturated fluids. However, there has been limited exploration into the interplay between the thermodynamic process of bubble formation and the dynamic equation governing the object's motion. In this paper, we present a comprehensive study of the oscillatory dynamics and mechanical behavior of an object immersed in a supersaturated fluid with time-varying bubbles on its surface, within a coupled thermodynamic-mechanical framework. We begin by proposing a macroscopic-scale model for nucleation; then, we integrate this nucleation process into the mechanical analysis of spherical objects; finally, we employ a mathematical model to elucidate the reasons and mechanisms behind these cyclical processes. We apply this model to quantitatively validate experimental outcomes under various initial conditions, demonstrating its theoretical, empirical, and statistical significance. This work provides a foundational theoretical basis for further research into the dynamics of gas-solid coupling systems and the complex behavior of particle movement within hydrodynamic environments.

1 Introduction **214**

2 Theoretical analysis **216**

2.1 Quantitative analysis **216**

*Award: 2024 S.-T. Yau High School Science Award (YHSA) Finale Bronze (Physics).
Instructor: Chengxin Zhang.

2.1.1 Nucleation rate 216
2.1.2 The vertical motion of the ball 217
2.1.3 Rotation 220
2.1.4 Combining translational and rotational motion 225
3 Empirical analysis 230
3.1 Experiment equipment 230
3.1.1 Determining nucleation rate 231
3.1.2 The rotation of the resin pellet 233
4 Summary and outlook 235
A Appendix A 237
A.1 Why our measurement for macroscopic nucleation rate is more accurate 237
A.2 Investigation into surface textures 238
A.3 Measuring nucleation rate at different temperatures 239
A.4 Determination of bubble size 240
A.5 Solving for pure rotational motion in Matlab (using ode45) 241
A.6 Solving coupled motion ODE in MATLAB (using ode15s) 245
Acknowledgments 251
References 252

1. Introduction

The formation of bubbles on submerged objects is fundamentally a process of heterogeneous nucleation: the surface of these objects offers varying numbers of nucleation sites depending on their roughness, enabling dissolved gas molecules that collide with the surface to adhere and accumulate. Different surface properties can lead to markedly different outcomes: when only soda is present in the beaker, bubbles formed on the smooth glass surface tend

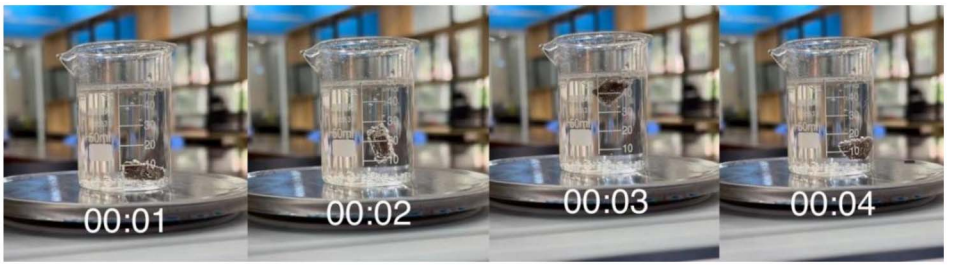

Figure 1: The image taken after the chocolate was put into the sparkling water for 1s, 2s, 3s and 4s respectively.

to detach rapidly; however, inserting a finger into the liquid causes bubbles to adhere swiftly and congregate on the skin. In contrast, dropping a Mentos candy, which has a significantly more porous surface, triggers a dramatic eruption. Only certain materials exhibit the "dancing" behavior. In our initial studies, we explored the oscillatory behavior of chocolate and raisins (as illustrated below, experiments can be conducted). Comparable phenomena have also been observed in chemical gardens, beer foam, and even volcanic eruptions [6]...

Numerous studies have explored various facets of these phenomena. In March 2023, Spagnolie et al. delved into the suspension and dynamics of objects within a saturated fluid [5], examining the intricate motion behaviors through both experimental and simulation approaches. That same year, A-Man Zhang et al. formulated a general theory on bubble evolution [7] and scrutinized the interactions among multiple bubbles. In 1959, Scriven et al. developed a mathematical model to describe microscopic nucleation in pure materials and binary mixtures [2]. In 2018, Soto et al. achieved precise control over the positioning and timing of bubble coalescence, conducting numerical simulations using the boundary integral method [4]. Additionally, in 1988, Lubetkin and Blackwel derived formulae to calculate the number of bubbles released from depressurized supersaturated fluids [1].

Historically, research has predominantly concentrated on bubble dynamics and simulation techniques, which, while showing qualitative agreement with experimental outcomes, have rarely probed the underlying coupling mechanisms within this thermodynamic-mechanical system involving gas, liquid, and solid phases. In contrast, our study specifically targeted and effectively characterized the coupled gas-fluid-solid system. We modeled the oscillatory motion of spherical objects within supersaturated fluids and validated our model through meticulously designed experiments.

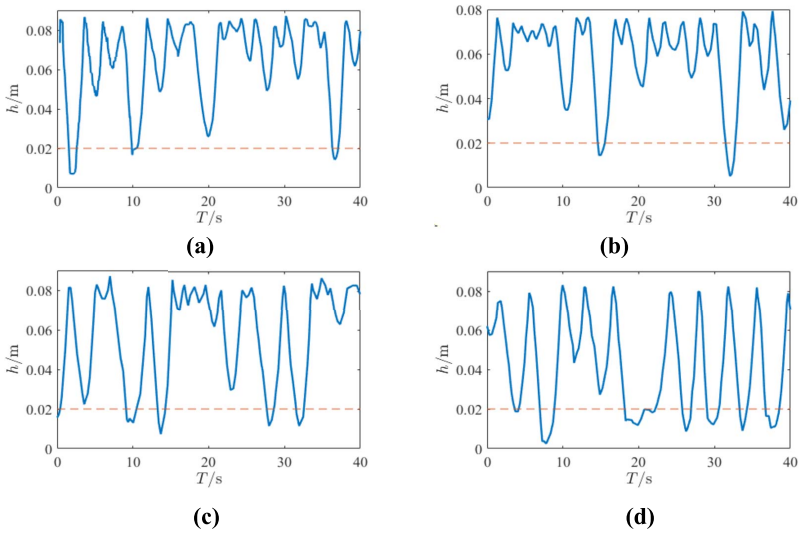

Figure 2: Vertical position of the chocolate vs time 5 minutes after immersion (a) 15 minutes (b), 25 minutes (c), and 35 minutes (d).

2. Theoretical analysis

2.1. Quantitative analysis

2.1.1. Nucleation rate. Bubble nucleation is influenced by numerous factors of the surrounding environment, the liquid, the gas and the submerged object, which, as proven by past attempts (CNT paper), are hard to quantitatively relate due to their complex interrelationships, especially when it comes to integrating microscopic properties into macroscopic dynamics (CNT paper). We incorporated the change of those properties into the change in buoyancy by looking into the change in nucleation rate as a function of time, avoiding possible variations that could happen due to reasons described above, and substantially simplifying the Classical Nucleation Model while maintaining the physical significance of descriptive variables.

We define the nucleation rate λ as the number of bubbles (N) formed per unit area (S_t) per unit time, where $\lambda = dN/S_t dt$, the variation of the number of bubbles satisfies

$$dN = \mu(S_t - S_0)dt \tag{1}$$

Where S_t is the total area of the attached surface, $S_0 = kN$ is the area occupied by bubbles. Assuming that the probability of nucleation is indepen-

dent of time per unoccupied area, that is, $d\mu/dt = 0$, then the differential equation for the change of the number of bubbles can be obtained as

$$\frac{dN}{dt} = \mu(S_t - kN) \tag{2}$$

By taking the time derivative of both sides of the equation

$$S_t \frac{d\lambda}{dt} = -\mu k S_t \lambda \tag{3}$$

Solving for λ, we get

$$\lambda = \lambda_0 \times \exp(-\mu k t) \tag{4}$$

Nucleation rate is obtained empirically, which we will elaborate on in part three. For resin material, nucleation rate is determined to be

$$\lambda = 2.309 \times 10^5 \times \exp\left(1.62 \times 10^{-3} \times t\right) \tag{5}$$

Once the formula describing the nucleation rate is obtained, it can be used to calculate the buoyancy of immersed objects in relation to time.

2.1.2. The vertical motion of the ball. In a supersaturated liquid, the forces on the sphere can be expressed separately as

$$G = mg \tag{6}$$

$$F_b = \rho_w g V_{tot} = \rho_w g \left(\frac{4\pi R_c^3}{3} + N(t)\,\overline{V}\right) \tag{7}$$

$$F_d = 6\pi\eta r v = 6\pi\eta R_c \frac{dy}{dt} \tag{8}$$

Assume that the downward direction is positive, we can write

$$\left(\rho_c \frac{4\pi R_c^3}{3}\right) \frac{d^2y}{dt^2} = \rho_c g \frac{4\pi R_c^3}{3} - 6\pi\eta R_c \frac{dy}{dt} - \rho_w g \left(\frac{4\pi R_c^3}{3} + N(t)\,\overline{V}\right) \tag{9}$$

Where ρ_c is the density of the ball, ρ_w is the density of the fluid, R_c is the radius of the ball, η is the viscosity coefficient, $N(t)$ is the number of adhering bubbles,$\overline{V} \equiv V_{tot}/N$ is the average volume of air bubble.

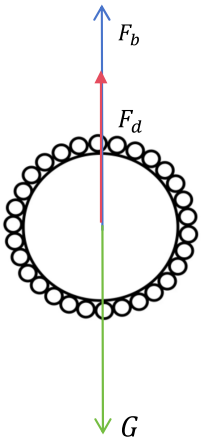

Figure 3: A 2-D free body diagram of an immersed sphere in supersaturated fluid viewed from the side of the container. The small circles represent bubbles, which do not necessarily bestrew the whole spherical surface.

Assume that the density of the liquid remains constant, then we define $\Theta \equiv \rho_w/\rho_c$, thus

$$\frac{d^2y}{dt^2} = (1-\Theta)\,g - \frac{9\eta}{2R_c^2\rho_c}\frac{dy}{dt} - \frac{3\Theta g N\,(t)\,\overline{V}}{R_c} \tag{10}$$

Substituting $\rho_c = 1.2\text{g/cm}^3$, $\rho_w = 1\text{g/cm}^3$, $\eta = 1.1 \times 10^{-3}\text{Pa} \cdot s$ at room temperature, $R_c = 0.01\text{m}$, $R_b = 6 \times 10^{-4}\text{m}$, setting initial acceleration and velocity of the immersed object to 0, and neglecting boundary conditions for now, we obtain the following graph:

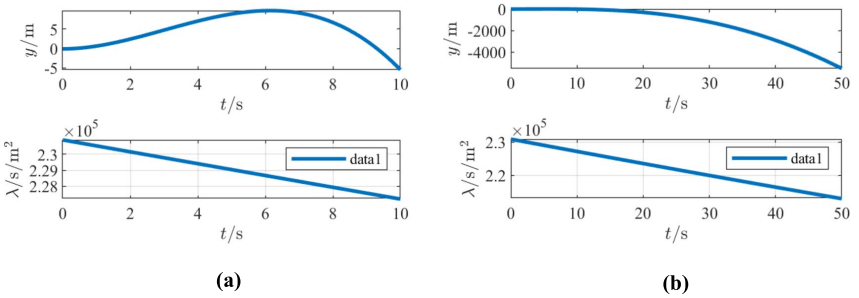

Figure 4: Vertical displacement of spherical resin within 10 seconds (a) and 5 seconds(b).

As can be seen, the resin sphere will sink for a short period of time due to gravity and then begin to ascend as buoyancy reaches a critical value at the absolute minimum of the h-t graph. Solving for that critical value using Newton's second law, we obtain

$$(1-\Theta)\, g = \frac{3\Theta g N\,(t)\,\overline{V}}{R_c} \tag{11}$$

The critical number of bubbles thus is

$$N_{threshold} = \frac{(1-\Theta)\, R_c}{3\Theta \overline{V}} \tag{12}$$

The conditions for oscillatory motion of the submerged object can also be derived

$$\Theta < \frac{R_c g}{R_c g + 3g\overline{V} \times \int_{t_1}^{t_2} \lambda(t) dt} \tag{13}$$

where $\int_{t_1}^{t_2} \lambda(t)$ is the number of bubbles formed from when the sphere is immersed. If any variables in this equation do not satisfy this condition, it is impossible for the sphere to ever oscillate.

Though it is a non-holonomic constraint of the system, the change of nucleation rate over time still greatly affects the movement of the pellets in bubble water. If the pellet is placed in carbonated water when it is first depressurized, as shown in Figure 5(a), since the nucleation rate is about$\lambda = 2.31 \times 10^5 \mathrm{m}^{-2}\mathrm{s}^{-1}$ it will soon ascend about 6 seconds after placement due to rapid bubble attachment. However, after ten minutes of depressurization, as

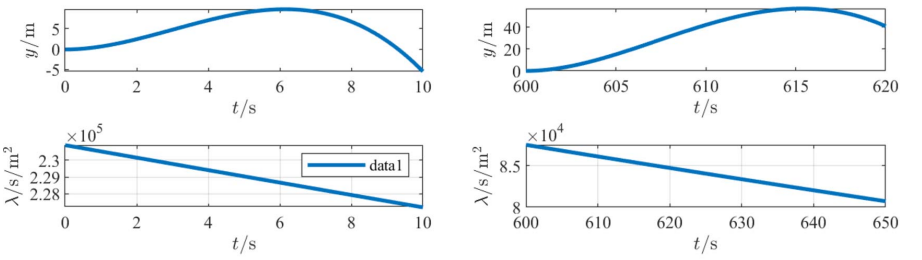

Figure 5: (a) shows the motion of the small ball when it is placed at t=0s; (b) shows the motion of the small ball when it is placed at t=600s.

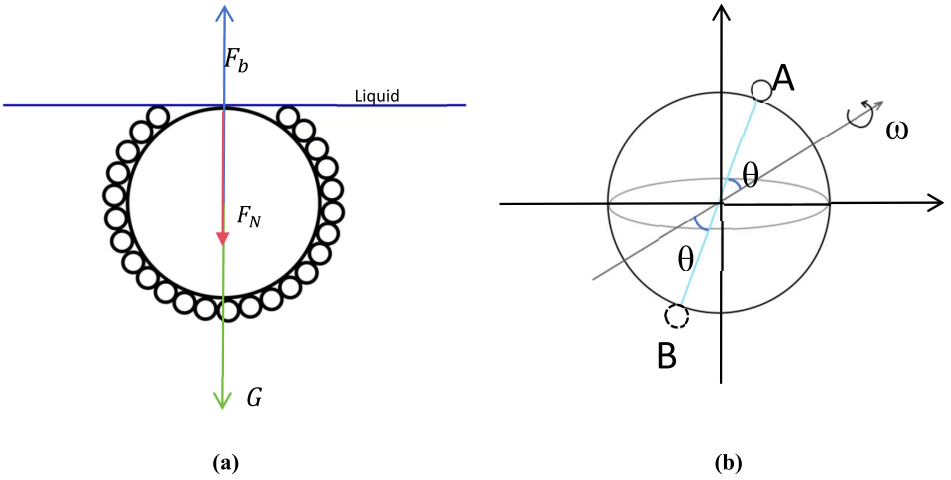

Figure 6: (a) Force analysis on the pellet at the liquid level. (b) The equivalent bubble on the surface of the sphere.

shown in Figure 5(b), it will take about 15 seconds before the bubbles reach the number needed to make the ball rise again.

2.1.3. Rotation. Bubble rupture is primarily triggered by object rotation at the fluid-air interface due to imbalanced torque. This rotation, in turn, leads to further changes in torque, which can either amplify or counterbalance the shearing forces acting on the sphere. The following sections will discuss in detail the chain burst reaction of bubbles resulting from this symmetry breaking.

Ideally, the effect of a bubble leaving or bursting can be regarded as equivalent to the formation of an additional bubble symmetric to the diameter of the sphere. Suppose the position of the bubble is (R_c, θ), then the torque of individual bubbles is

$$\tau_b = -f_b R_c \cos\theta \tag{14}$$

Where $f_b = F_b/N = \rho_w g\overline{V}$ is the buoyancy force of a single bubble. The mechanism by which the ball starts to spin is usually triggered by a random perturbation caused by rising bubbles or by bubble detachment. This perturbation may determine whether the ball oscillates and stays on the surface or spins and sinks. In this process, the top of the ball is in contact with the liquid surface but not exposed. According to geometry shown in Figure

7(a), each bubble occupies a solid angle of $4R_b^2/R_c^2$. When assuming a single rotational axis and in 2 dimensions ($R_b \ll R_c$), it can be simplified to $\theta_b \approx \tan\theta_b = 2R_b/(R_c + R_b)$, which has been essentially verified experimentally. As such, bubbles touching the liquid surface will be driven to burst with each unit angle of rotation, forming an approximately rectangular empty belt, as shown in Figure 7(b).

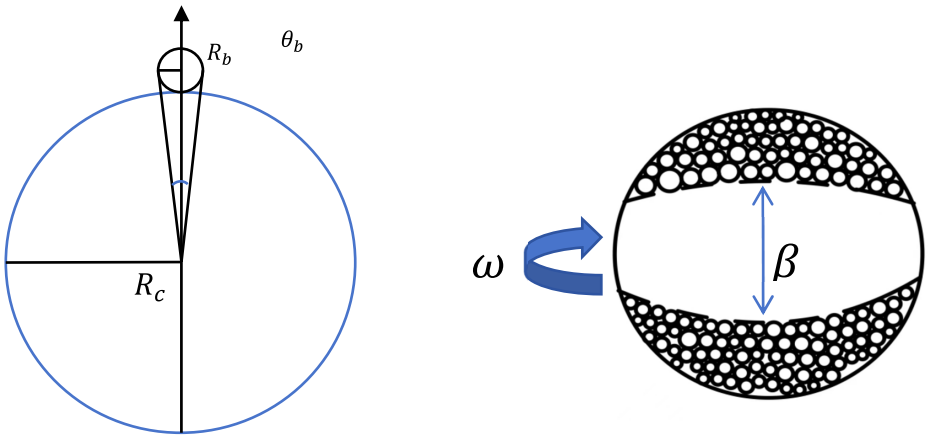

Figure 7: (a) shows the schematic diagram of the Angle occupied by a bubble θ_b. (b) shows the schematic diagram of an almost rectangular empty band caused by rotation.

Which occupies an angle of

$$\beta = \left\lceil 2\cos^{-1}\left(\frac{R_c}{R_c + R_b}\right)\right\rceil \tag{15}$$

Corresponding number of bubbles on the width of this rectangular belt is therefore $N_{width} = \beta/\theta_b$.

Now we are equipped to discuss the chain reaction.

The total torque generated by the bubble bursting driven by the perturbation can be written as

$$\begin{aligned}\tau_{break} &= -F_{de}R_c\cos\theta_0 + \sum_{i=0}^{N_{break}} -F_bR_c\cos(\frac{\pi}{2} + i\theta_b) \\ &= -F_{de}R_c\cos\theta_0 + \sum_{i=0}^{N_{break}} \mathrm{F_b}R_c\sin(i\theta_b)\end{aligned} \tag{16}$$

Where N_{break} is the number of bubbles broken, F_{de} is the magnitude perturbation force, θ_0 is its angular position. Since $\ddot{\theta}_{break} = \tau_{break}/I_c$, where $I_c = 2M_cR_c^2/5$, and

$$\omega_{break} = \int_0^t \ddot{\theta}_{break} dt.$$

We can integrate to get the angle of rotation caused by the angular velocity, and thus the number of bubbles broken as a result of solely the perturbation is

$$N_{break} = \left\lceil \frac{1}{\theta_b} \int_0^t \omega_{break} dt \right\rceil \tag{17}$$

rounded up because a bubble is assumed to break upon contact with the fluid surface.

We also need to take into account the moment of rotation due to bubble reformation. These turning moments are important for near-surface oscillations. We define S_a as the empty area available for bubble formation:

$$S_a = N_{break} \cdot S_b - N_{new} \cdot S_b \tag{18}$$

where $N_{new} = \left\lceil \int_0^t \lambda dt \cdot \int_0^t dS_a(t')\ dt' \right\rceil$ is the number of new bubbles formed on the previous available area.

Therefore

$$S_a = \frac{N_{break} \cdot S_b}{1 + \int_0^t \lambda dt \cdot S_b} \tag{19}$$

Since new bubbles form in chronological order, their moment can be written as

$$\tau_{new} = \sum_{j=0}^{N_{new}} F_b R_c \cos\left(\frac{\pi}{2} + \theta - j\theta_b\right) = \sum_{j=0}^{N_{new}} F_b R_c \sin\left(\theta - j\theta_b\right) \tag{20}$$

The net instantaneous angular acceleration, then, is the resultant moment divided by the moment of inertia of the ball

(21)

$$\ddot{\theta} = \frac{\tau_{break} + \tau_{new}}{I_c} = \frac{-F_b\left(\cos\theta - \sum_{i=0}^{N_{break}} \sin(i\theta_b) + \sum_{j=0}^{N_{new}} \sin\left(\theta - j\theta_b\right)\right)}{\frac{2}{5} M_c R_c}$$

And the total amount of bubbles broken is $N_{tot} = (N_{new} - N_{break}) \cdot N_{width}$

A series of observed phenomena can be explained by this model. We observe that after reaching the surface of the liquid, the submerged object sometimes rotates slightly back and forth on the surface, finally settling down and continuing to float, and other times it rotates more violently and begins to sink, but to different depths. This is due to the different locations where perturbations occur. And according to equation (14), when $|\tau_b|$is the largest, the angular position of the same magnitude of perturbation is either $\theta_0 = 0$ or $\theta_0 = \pi$, meaning that perturbations at the equator of the sphere will bring about the most obvious rotation effect, while the disturbances near the top and bottom of the sphere crown will only cause slight oscillation. We also observed that when they reach a certain extent, the bubble is unable to support its continued to float due to induced rotation; that is because $(N_{new} - N_{break}) \cdot N_{width} = N_{tot} \geq N_{thresh}$, where$N_{thresh}$ is the maximum number of bubbles when the ball sinks.

Due to the difficulty of obtaining analytical solutions for these equations, which we attempted to solve using the Poincaré–Lindstedt method, we employed the Runge-Kutta method and Gear's method in MATLAB to obtain accurate numerical solutions for the angular velocity and the net number of bubbles broken under different initial perturbations.

Suppose that the perturbation is the torque generated when a bubble bursts, as shown in FIG. 8(a) and 8(b), when the position generated by the perturbation is at a 90-degree angle with respect to the horizontal axis passing through the center of the ball, the moment balance of the ball will not be broken, therefore, the net rupture amount of the bubble N_{broken} and the angular velocity of the ball are always zero. As shown in FIG. 8(c) and FIG. 8(d), when the position generated by the perturbation is 0 degrees from the axis passing through the spherical center horizontally, that is, it is just at the equator of the pellet, the pellet will oscillate, and the net burst amount of the bubble per second will increase or decrease periodically, until the integral of the total burst amount reaches 0 around $t = 1.6$s, and the bubble will cover the surface of the pellet again. Because the perturbation here is assumed to be very small, in an ideal situation, even if a bubble bursts at the position with the greatest torque, it will not cause the ball to fall. In practice, however, it is reasonable to assume that in the total ideal situation, even if a bubble bursts at the position with the greatest torque, it will not cause the ball to fall, and that the angular velocity and rotation angle have a small initial value due to the momentum generated by touching the liquid surface.

Figure 9 shows a very non-linear and seemingly non-periodic but oscillatory relationship between N_{new} and N_{broken}, the rate at which bubbles form and break on the sphere's surface. Qualitatively, the fluid-air surface is a place

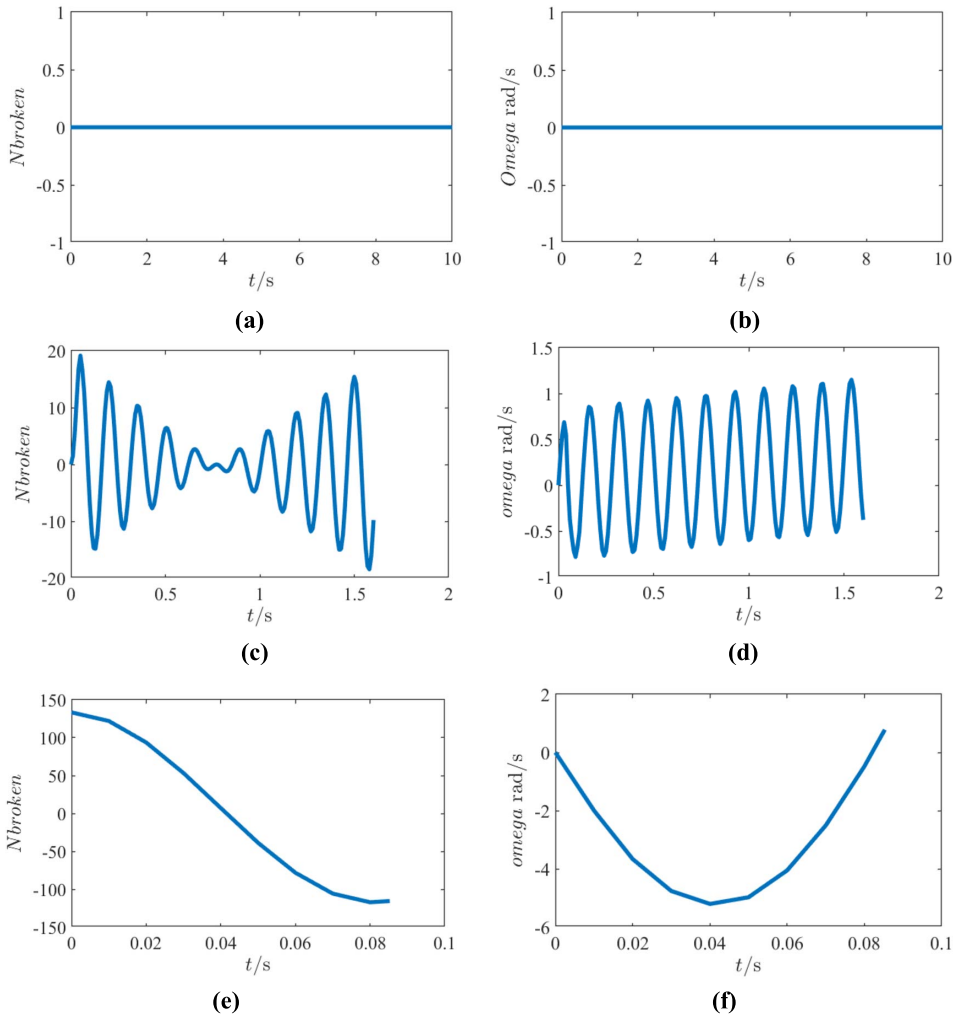

Figure 8: The relationship between the bubble burst quantity and angular velocity with time obtained after solving equation (21) with different initial conditions. N_{broken} the number of bubbles broken, and the positive direction of ω is clockwise. In the figure, the parameters taken are as follows: $\Theta = 1.0(\mathrm{g/cm^3})/1.2(\mathrm{g/cm^3}) = 0.83$, $R_c = 0.01\mathrm{m}$, $R_b = 0.0006\mathrm{m}$. Calculated by (13), we can found that θ_b=$2R_b/(R_c + R_b)$=$0.21°$, $N_{width} = 25$.

of equilibrium for the sphere at certain nucleation rates, but the equilibrium state is constantly disturbed by random perturbations. The solutions of the differential equations show that not only the disturbances are random, but

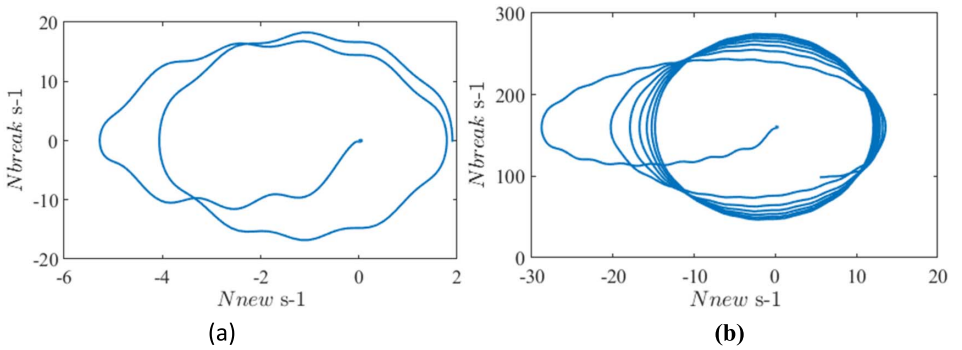

Figure 9: (a) N_{new} vs N_{broken} for the second case in figure 8. (b) N_{new} vs N_{broken} for the third case in figure 8.

also their subsequent results. This is why the motion of objects in carbonated water doesn't have a periodic nature and is so hard to predict in a prolonged observational interval.

2.1.4. Combining translational and rotational motion. An oscillatory period consists of four stages: resting at the bottom, ascending, floating, and descending. Throughout the stationary and ascending phases, the movement of the chocolate is predominantly governed by the rate of bubble formation. While the chocolate remains at rest, bubbles continue to emerge on its surface until the buoyant force exceeds the gravitational pull, prompting the chocolate to rise. Upon reaching the liquid's surface, vertical movement ceases until the threshold Nthresh is attained, at which point gravity once more prevails over buoyancy. To fully describe the "dancing" period, one must detail how the quantity of bubbles (which dictates translational acceleration) and their position (which dictates angular acceleration) interact and affect the object's motion at various stages.

When only translation is considered, the total bubble adhesion is defined as the integral of nucleation rate over time and area. Now, the combination of translation and rotation is used. $N(t) = \int_{t_1}^{t_2} \lambda(t)dt$ in the suspended state, and the rotational pair of bubbles is considered at the boundary 1. The difference caused by number is that bubbles may not cover all the surface of the ball when the ball collides with the liquid surface. Therefore, the area of bubbles that can be attached S_a is not only the area swept by rotation, but also the area not occupied during bubble accumulation when rising. The column can

therefore be written as follows:

$$\begin{aligned} S_a &= S_{total} - N_{new}S_b + N_{break} \cdot S_b \\ &= S_{total} - (\left\lceil \int_0^t \lambda(t)dt \cdot S_a \right\rceil - N_{break})S_b \\ &= \frac{S_{total} + N_{break}S_b}{1 + \int_0^t \lambda(t)dtS_b} \end{aligned} \tag{22}$$

Here S_{total} is the total surface area of the ball, and since new bubbles only form on S_a, therefore

$$\begin{aligned} N_{new} &= \int_0^t \lambda(t)dt \cdot S_a \\ &= \int_0^t \lambda(t)dt \frac{S_{total} + N_{break}S_b}{1 + \int_0^t \lambda(t)dtS_b} \end{aligned} \tag{23}$$

Bring in the formula for the total bubble burst

$$N_{tot} = (N_{break} - N_{new}) \cdot N_{width} \tag{24}$$

After plugging in the formula (23)

$$N_{tot} = N_{width} \int_0^t \lambda\left(t\right) dt \left(\frac{N_{break}\left(1 + \int_0^t \lambda\left(t\right) dtS_b - S_b\right) - S_{total}}{1 + \int_0^t \lambda\left(t\right) dtS_b} \right) \tag{25}$$

And the total bubble attachment amount controlling the buoyancy change in the translational formula is equal to the maximum bubble amount at full time minus the total burst bubble amount

$$N_{net} = \frac{4\pi R_c^2}{S_b} - N_{tot} \tag{26}$$

Plugging this into formula (25)

(27)

$$N_{net} = \frac{4\pi R_c^2}{S_b} - N_{width} \int_0^t \lambda(t)dt \left(\frac{N_{break}\left(1 + \int_0^t \lambda(t)dtS_b - S_b\right) - S_{total}}{1 + \int_0^t \lambda(t)dtS_b} \right)$$

Using ode15s, which is especially designed for stiff problems like this, to solve for numerical solutions, we obtain the following results:

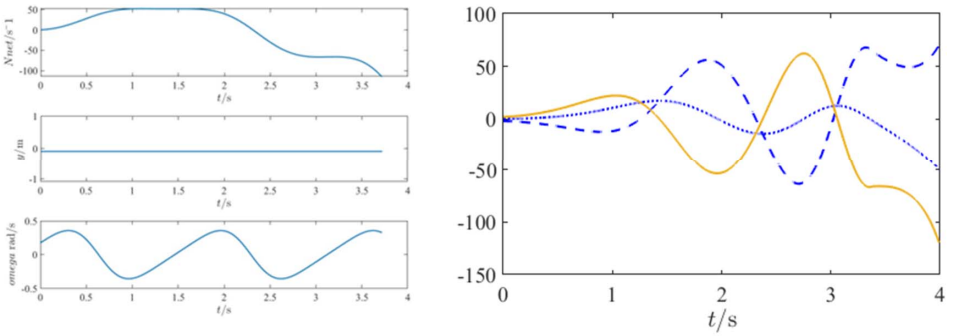

(a) (b)

Figure 10: The numerical solution coupling the rotational and translational motion of a resin sphere inside carbonated water when given a perturbation of 0.5rad/s^2. In this figure, the parameters taken are as follows: sphere density $\rho_c = 1.2$g/cm^3, radius of sphere $R_c = 0.01$m,, radius of bubble $R_b = 0.0006$m, and the initial number of bubbles is set to 1000. Calculated by type (13) θ_b=$2R_b/(R_c+R_b)$=0.21°, $N_{width} = 25$. Figure (a) shows the net rate of bubble rupturing, the vertical position, and the net angular velocity of the resin sphere at perturbations of 0.5rad/s^2. Figure (b) shows the separate number of ruptured bubbles(yellow solid line), newly formed bubbles (blue dotted line), and the total amount of bubbles formed, which is the time integral of N_{net}(blue dashed line) at each second. Calculation is terminated when the sphere is set to back to rotational equilibrium.

It can be seen that when perturbation is small, the initial amount of bubbles is enough for the ball to remain on the liquid surface, and the nucleation rate of bubbles is greater than the breaking rate, so the surface of the ball will soon be filled with bubbles again after a slight oscillation. During the oscillation, as new bubbles gradually covers the whole surface again, the amount of new bubbles formed each second gradually approaches zero while the sphere approaches its equilibrium.

Setting the perturbation to a larger value of 10rad/s^2, we can see more bubbles broken as a result of the chain effect subsequent to the initial fluctuation. More ruptured bubbles also gives space for more bubbles to nucleate (greater S_a). Thus, although there is significant increase in angular velocity and bubble rupturing rate, the ball can still manage to stay at the fluid-air interface.

When the perturbation is large enough, however, the ball will immediately break away from the fluid-air interface and start to sink. The total

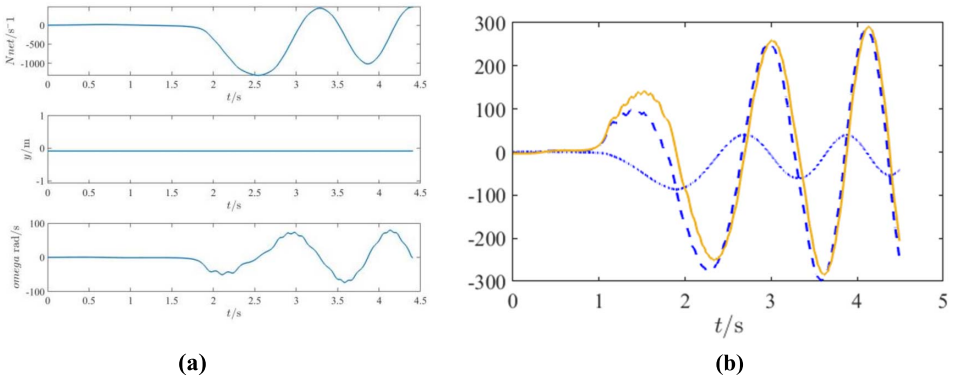

Figure 11: The numerical solution coupling the rotational and translational motion of a resin sphere inside carbonated water when given a perturbation of 10rad/s^2.

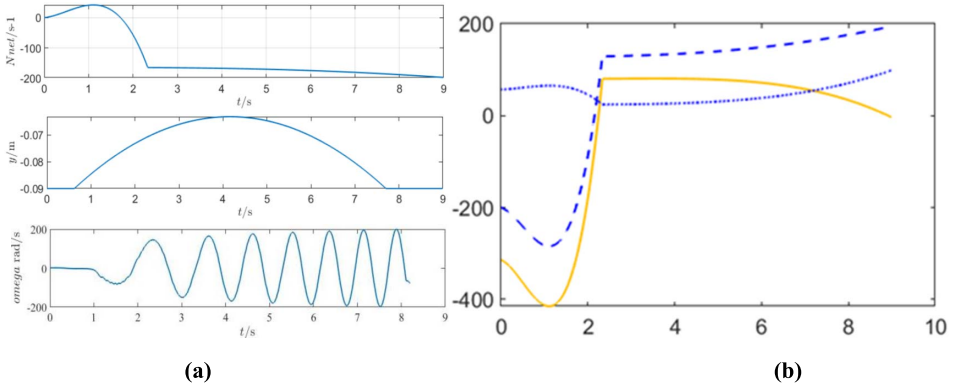

Figure 12: The numerical solution coupling the rotational and translational motion of a resin sphere inside carbonated water when given a perturbation of 100rad/s^2.

bubble increment per unit time is maintained as the nucleation rate, and the newly formed bubble will produce a moment that keeps the ball rotating while sinking. Once the ball leaves the fluid-air interface, the only variable that dominates the number of bubbles adhering to its surface is nucleation, which is shown by the dotted blue line incrementing after 2.33 seconds, which eventually let the ball to reach another rotational equilibrium.

In this case of vertical motion domination, the relationship between Nbreak and Nnew is approximately linear, as the nucleation rate in a short

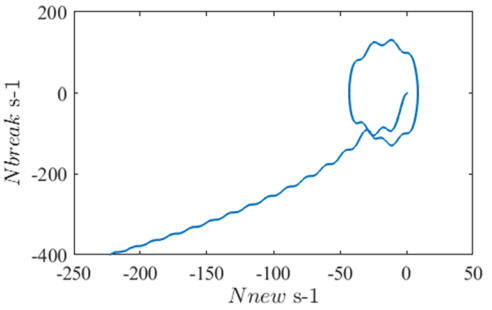

Figure 13: The phase plane of the rate of bubbles broken as a function of the rate of bubbles forming per unit time. Quantization of bubbles (forming one by one) can be seen clearly from this graph.

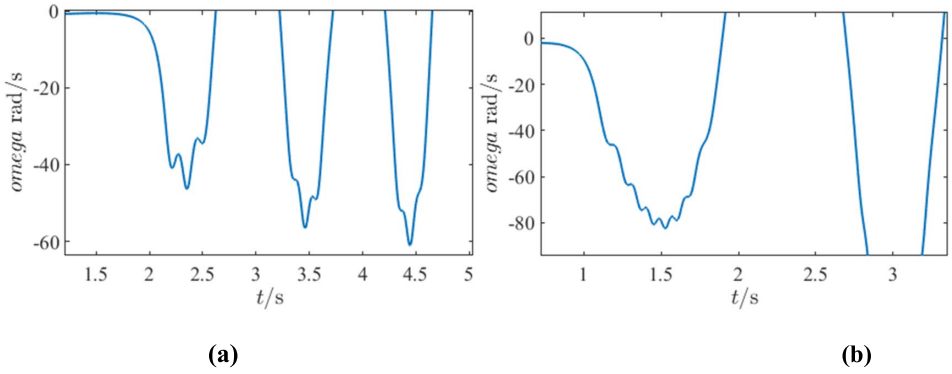

Figure 14: A zoomed-in graph of the numerical solution of the angular velocity of the resin sphere, showing the "bumps" created by the returning torques of the newly formed bubbles. (a) angular velocity given perturbation =10rad/s^2 (b) angular velocity given perturbation =100rad/s^2.

time period (9seconds), with small oscillatory fluctuations due to the quantized nature of bubbles. This shows the dominance of nucleation rate during vertical motion. But as soon as the resin sphere reaches the fluid-air interface, the relationship between Nbreak returns to an intertwined relationship as discussed in former parts.

Note that there are small "bumps" on the graph of the angular velocity, which clearly show the turning moments exhibited by the freshly formed bubbles. The greater the initial perturbation, the more new bubbles will form, making the "bumps" more obvious, which is also validated empirically after deriving the formula.

3. Empirical analysis

3.1. Experiment equipment

To prepare the supersaturated carbonated water, we made sure to keep a constant supersaturation ratio and at a fixed pressure: we used a saturator to inject a fixed amount(7.5g) of CO2 kept in cartridge through a dosing nozzle into one liter of water. As the saturator has an uneven container, we instead used a cylindrical beaker with a base radius of R= 3.5cm and a volume of 300mL, in which the carbonated water is poured carefully down the inner wall of container to a height of 9cm.

We used a 3D printed resin sphere of radius 0.5cm and a mass of 0.6g to determine the nucleation rate on resin material and to examine the nucleation rate and object motion at room temperature and at different temperatures (achieved by using a heater). We used 3D printed resin spheres of different sizes ($R_c = 0.25cm$, $R_c = 0.5cm$, $R_c = 1cm$) to examine the motion of

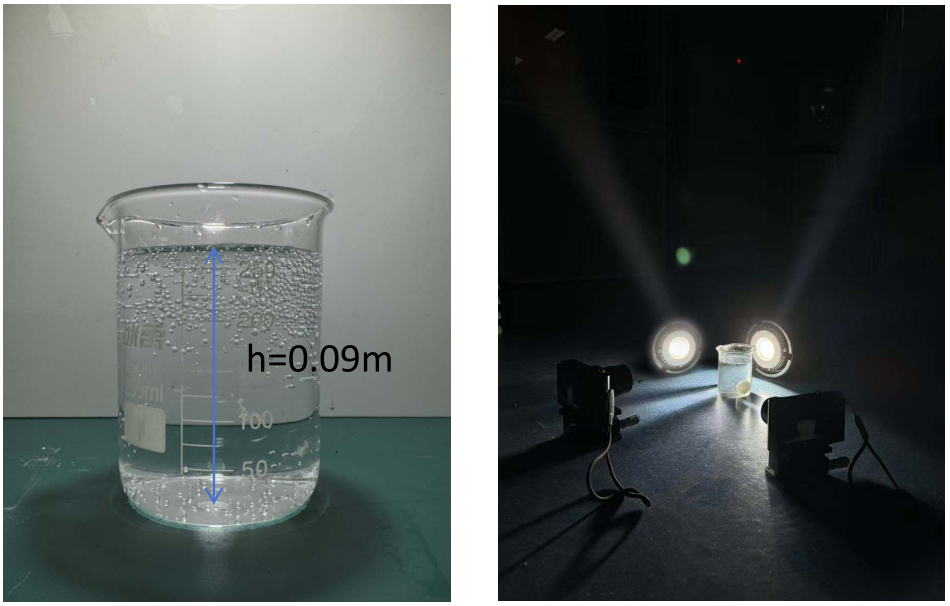

(a) (b)

Figure 15: (a) Experimental setup used to measure nucleation rate, translational motion, and coupled motions (b) Experimental setup used to capture bubble-cleaning rotation at the fluid-air interface.

objects of different mass-to-surface-area ratio with the same nucleation rate function. We used balls of approximately the same mass and size but made of different materials to examine their oscillatory behaviors.

When recording the translational movement and the oscillatory motion as a whole, we used the built-in camera of iPad pro at 30 frames per second. When examining rotational motion at the fluid-air interface, we used two high-speed Sony Alpha7 iii cameras arranged orthometrically to reconstruct their dynamic properties.

3.1.1. Determining nucleation rate. Since nucleation rate is defined as the number of bubbles formed per unit time per unit area, determining the specific number of bubbles at different chronological intervals on a known surface area would provide sufficient data to fit a curve of nucleation rate as a function of time. We started timing as soon as carbonated water was poured into the beaker, and we drop the resin ball with no initial velocity into the carbonated water once every 30 seconds and recorded the time between when the ball was immersed and when it started to rise. The time needed for the sphere to rise τ is plotted as a function of time as shown in Figure 16. During this time interval τ where buoyancy gradually balances out gravity, and the number of bubbles increases from zero to Nthreshold (in this case is approximately 116 bubbles according to equation #12) on a surface area of $3.14 \times 10^{-4}\mathrm{m}^2$.

Since the mass and surface area of the pellet are known, we obtained the fitted curve of the nucleation rate using $\lambda = \frac{[\mathrm{N(t)}/4\pi\mathrm{R}^2]}{\tau}$ from equation 11, with

$$N\left(t\right) = \left(1 - \Theta\right) R_c / 3\Theta\overline{V} = 2.68 \times 10^5 \mathrm{m}^{-2}.$$

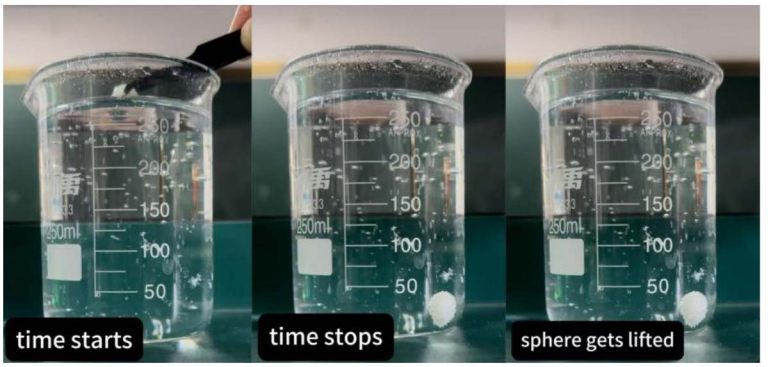

Figure 16: Method for nucleation rate determination.

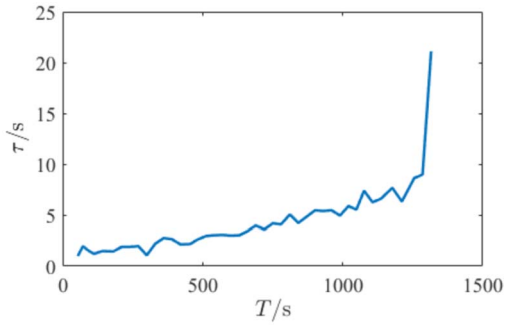

Figure 17: The variation of the time interval τ required for the resin sphere to sink and then start to float with the placement time T of the carbonated water.

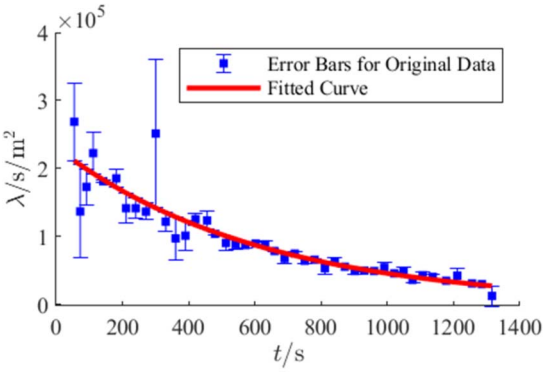

Figure 18: Contrast images of fitted curves and experimental data.

Fitting in the MATLAB fitting toolbox, we found that the nucleation rate is $\lambda = 2.309 \times 10^5 \times \exp(-1.62 \times 10^{-3}t)$. The exponential form of this equation is consistent with our theoretical prediction.

Using the variance $\mathrm{SE} = \sqrt{\frac{1}{\mathrm{N}-1}\sum_{\mathrm{i}=1}^{\mathrm{N}}(\mathrm{R_i} - \mathrm{R_{fitted}})^2}$ as the error value, we plotted the fitting results in blue circles in Figure 15.

The form of the fitted function if consistent with our theoretical prediction for nucleation rate, and the fitting result also shows a coefficient of determination R^2=0.8347, indicating that the fitted image explains more than 83% of the data points and has a high degree of fitting. As with Saverio et al, the fitting result of their data with their proposed nucleation rate as a function of supersaturation ratio is only 0.3048. This notable discrepancy is probably due to experimental fallacies discussed in the appendix.

3.1.2. The rotation of the resin pellet. There are several difficulties in measuring the rotational motion of the sphere at the fluid-air interface. Firstly, in most cases, the sphere does not exhibit only rotational motion at the fluid-air interface, but instead rotate while moving its center of mass around. Secondly, accurately capturing three-dimensional rotation is difficult when using only a single recording device. To resolve those difficulties, we set up two orthometric high-speed cameras to capture the motion in the x-y plane and y-z plane separately and reconstruct them using simple geometry (Figure 19).

With (x1, y1), (x2, y2) representing the position of a marked point on the surface of the spherical resin at two different points in time for the first camera, and (x1, y1), (x2, y2) representing the position of a same marked point on the surface of the spherical resin at two different times for the second camera, l and l' each represent the distance traveled by the center of mass of the resin sphere for the two cameras.

For each camera's visual plane,

$$\Delta\theta = \frac{\sqrt{(x_2 - l - x_1)^2 + (y_2 - y_1)^2}}{R_c} \tag{28}$$

$$\Delta\theta' = \frac{\sqrt{(x_2' - l' - x_1')^2 + (y_2' - y_1')^2}}{R_c} \tag{29}$$

The total angular displacement is therefore the vector sum of the two:

$$\Delta\theta_{total} = \frac{\sqrt{(x_2' - l' - x_1')^2 + (y_2' - y_1')^2 + (x_2 - l - x_1)^2 + (y_2 - y_1)^2}}{R_c} \tag{30}$$

The angular velocity and acceleration can be calculated by taking the time derivative of $\Delta\theta_{total}$, with Δt depending on the time lapse in Tracker.

Measuring the angular velocity of the sphere using this method, we obtained the following diagrams for angular displacement θ and velocity ω (Figures 20 and 21).

It can be seen that when the perturbation is relatively small, about $6.06\mathbf{rad/s^2}$, the sphere wobbles on the fluid-air interface. However, when the perturbation is larger, measured to be about $101.18\mathbf{rad/s^2}$, the sphere exhibits more significant and irregular rotation while starting to plummet. These observed phenomena are consistent with our theoretical predictions which are shown in the figures drawn in blue.

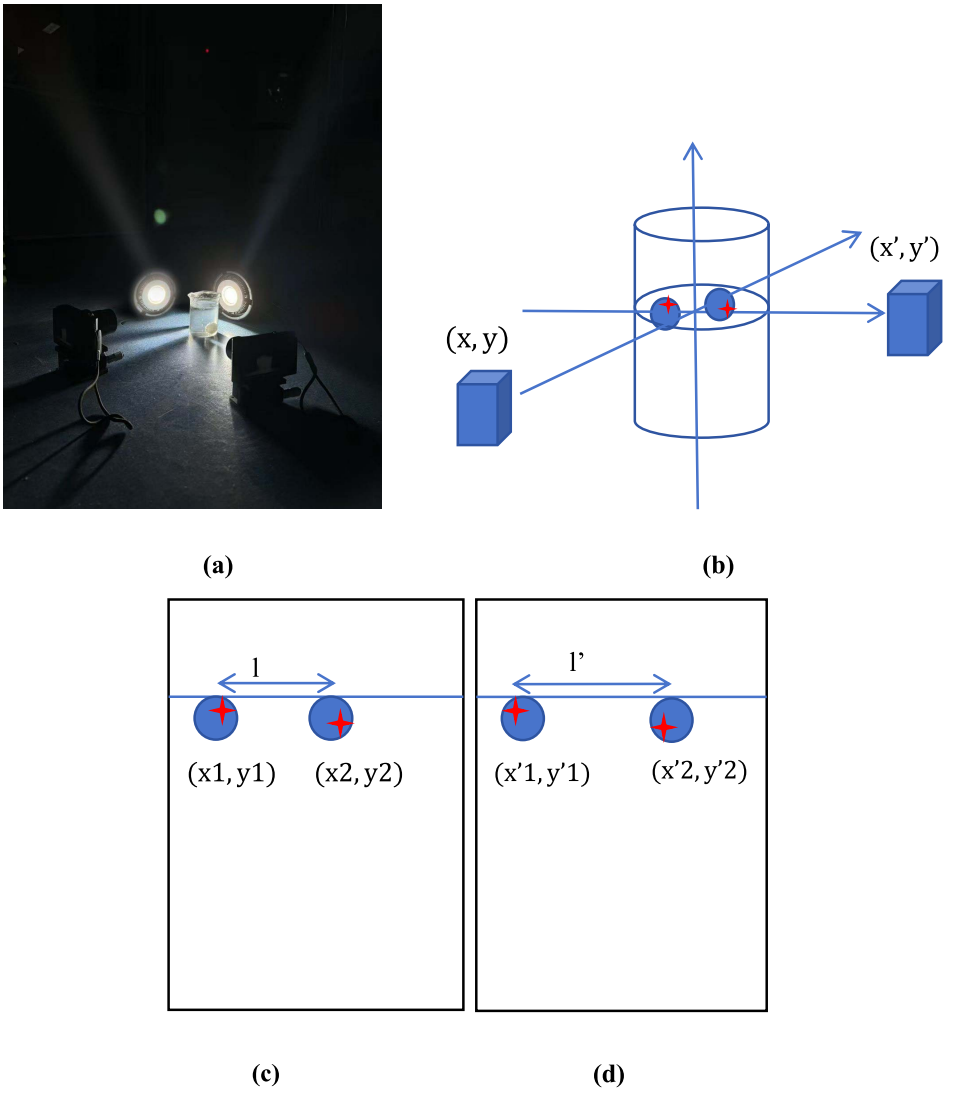

Figure 19: Experimental configuration for rotational motion measurement. The two spheres represent the submerged object at different points in time, while the red cross indicates a fixed point on the sphere used to track its rotation. (a) is the real experimental setup, and (b) is the three-dimensional scheme of the setup, indicating the coordinate system used by each shooting device. (c) and (d) are the views of the second camera.

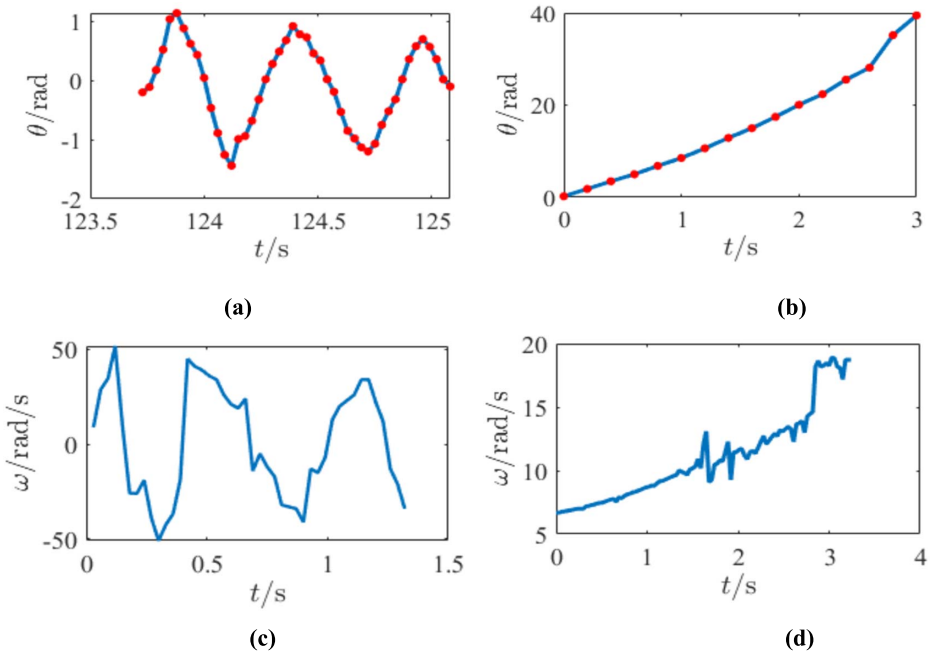

Figure 20: The angular displacement and velocity when initial perturbation is 6.06rad/s^2 for (a)(c) and 101.18rad/s^2(b)(d).

4. Summary and outlook

We have developed a comprehensive framework that successfully predicts the dynamic behavior of objects in a gas-solid coupled system, particularly within the context of sinking and floating phenomena observed in supersaturated fluid. The framework is based on a macro-scale model of gas nucleation, which is quantitatively analyzed to determine the rate at which bubbles form on the surface of submerged objects. This rate is a critical factor in understanding the vertical motion of the objects, which is further influenced by forces such as gravity, buoyancy, viscous drag and surface tension. Our model also accounts for the chain effect of the bubble-cleaning rotational motion of objects at the fluid-air interface, triggered by the perturbations from random bubble rupture or detachment. Numerical simulations, utilizing methods such as the Runge-Kutta algorithm and Gear's methods (backward differentiation formulas) are employed to solve the stiff ordinary differential equations of the object's dynamic behavior, and provide accurate predictions of the system's behavior.

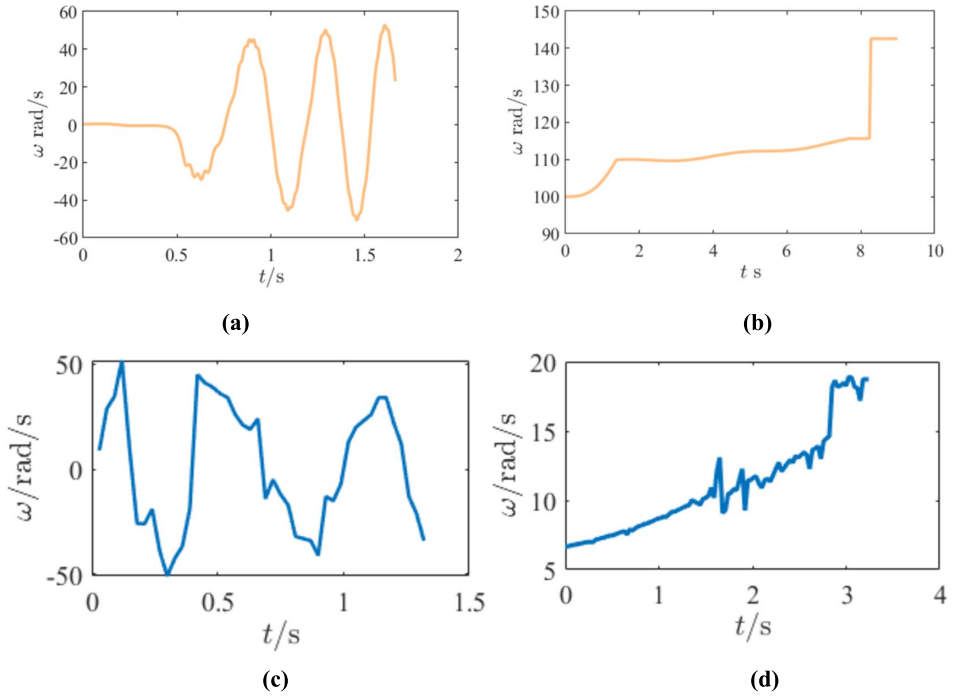

Figure 21: The modeled angular velocity versus experimental data with the same initial conditions as Figure 20.

The theoretical findings are validated through meticulous experiments involving orthometric high-speed shooting system and controlled supersaturation ratio environments. The seamless integration of experimental data with theoretical predictions solidifies the model's reliability and applicability in various hydrodynamic scenarios.

Our research paves the way for potential advancements in the study of coupled self-propelled non-equilibrium thermodynamic and dynamic systems such as those for active matter, where systems exhibit complex, collective behaviors driven by interrelated factors. Our research's ability to predict and control the motion of objects in fluid environments implied that our approach can be further applied to explore the stability and phase transition behaviors of active matter under different conditions like the design of micro-robots, environmental monitoring, and the understanding of natural phenomena such as volcanic eruptions and chemical gardens. Future work could explore the extension of this model to more intricate systems, including the effects of varying surface properties and the integration of external forces like magnetic

or electric fields. Additionally, the potential applications of our research in medicine, environmental science, and materials engineering are vast, offering a promising avenue for interdisciplinary innovation.

Appendix A

A.1. Why our measurement for macroscopic nucleation rate is more accurate

Other's method:

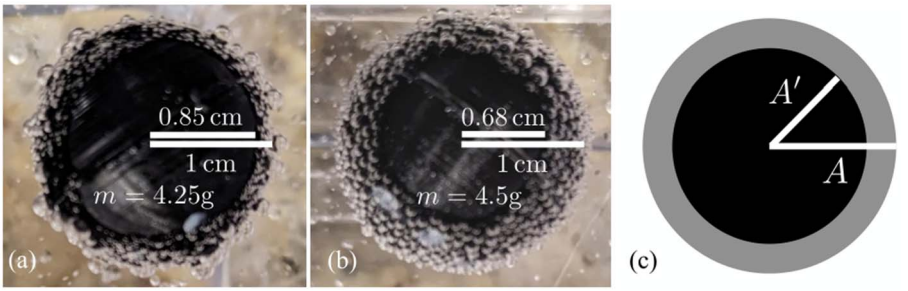

Figure 22: Measurement method mentioned in other research papers.

"Estimating the lifting force using body emergence. (a) A lighter body is pushed further out of the fluid by surface bubbles. (b) A heavier body presents less of its surface to the air, and bubble-cleaning rotations become more important. (c) [Buoyancy change] can be reasonably (under-)estimated during the body's brief visit to the surface by measuring the radial distance A' where the body reenters the fluid, as viewed from above." [5]

The underestimation mentioned happens because of the upthrust of the spherical object. This experimental method of measuring radial distance where the body reenters the liquid has several other possible disadvantaged:

1. It is hard to determine the exact radius of of reentering when viewed from above
2. It only applies for situations where bodies do emerge from the liquid, which is not true for all situations we observe.
3. It is limited to measure buoyancy change for spherical objects

By determining the mid-fluid buoyancy and measuring time taken for the bubbles to reach the minimum number essential for reaching that number, our method meticulously resolved the problems mentioned using simple equipment, as shown in part 3.1.1.

A.2. Investigation into surface textures

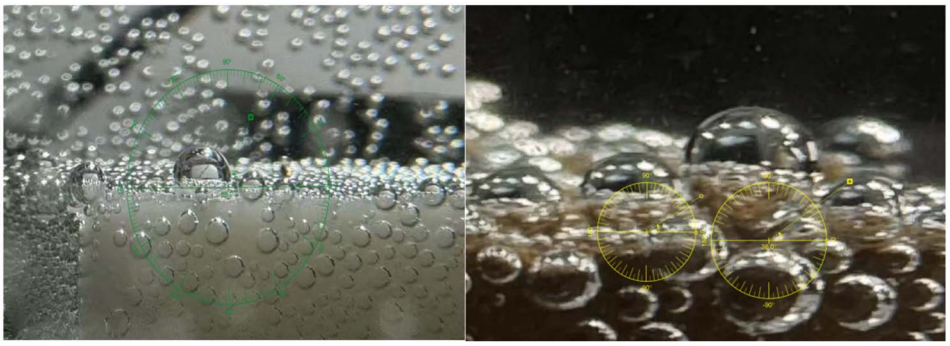

Figure 23: (a) carbon dioxide bubbles on resin (b) carbon dioxide bubbles on resin. We measured the contact angle of gas bubbles by the conventional way of measuring liquid contact angle, and we took the mean value of all 15 contact angles measure to get an approximated contact angle for each material.

We used resin and chocolate spheres of the same size (R=0.5cm) to examine the nucleation rate of carbon dioxide on different surface textures, which are demonstrated by contact angles. We measured the mean contact angle of resin to be 116.81° and the mean contact angle of chocolate to be 144.27°. since $144.27° > 116.81°$, gas is more likely to attach to the surface of resin than chocolate, meaning that chocolate is likely going to have a smaller value of μ and a smaller initial nucleation rate λ_0.

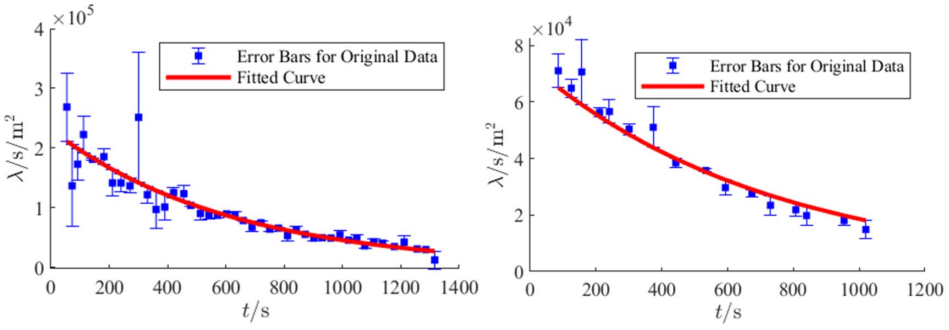

Figure 24: (a) nucleation rate for resin at room temperature (20°C), (b) nucleation rate for chocolate at room temperature.

Our measured nucleation rate aligned with this: for resin, $\lambda_{\text{resin}} = 7.314 \times 10^4 \times exp(-1.37 \times 10^{-3}t)$, for chocolate, $\lambda_{\text{chocolate}}=2.309 \times 10^5 \times exp(-1.62 \times 10^{-3}t)$, which has a higher initial nucleation rate and bubble-forming probability.

A.3. Measuring nucleation rate at different temperatures

We compared the nucleation rate of carbon dioxide on resin at room temperature and at 40°C, which we managed to heat to and preserve at for as long as our experiments went with an electronic kettle.

We found that nucleation rate changed from $2.309 \times 10^5 \times \exp(-1.62 \times 10^{-3}t)$ to $3.110 \times 10^4 \times \exp(-1.58 \times 10^{-3}t)$. It is worth noting that while initial nucleation rate decreased significantly when heated, the probability for bubble formation on a fixed surface almost stayed constant (-1.62×10^{-3} vs -1.58×10^{-3}). This supports our theory: the probability of bubble formation on a fixed surface depends solely on the texture of the nucleation site, while the initial nucleation rate is influenced by external factors such as temperature and pressure.

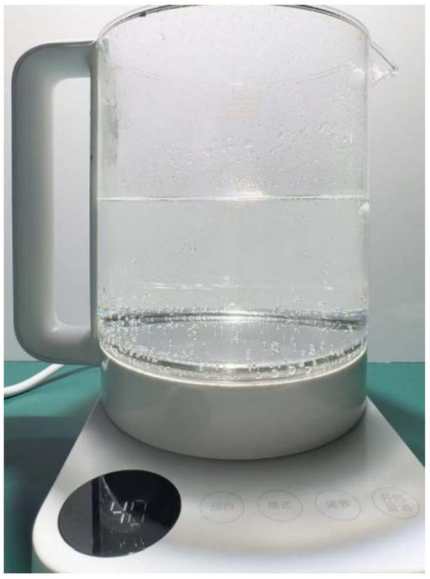

Figure 25: The kettle.

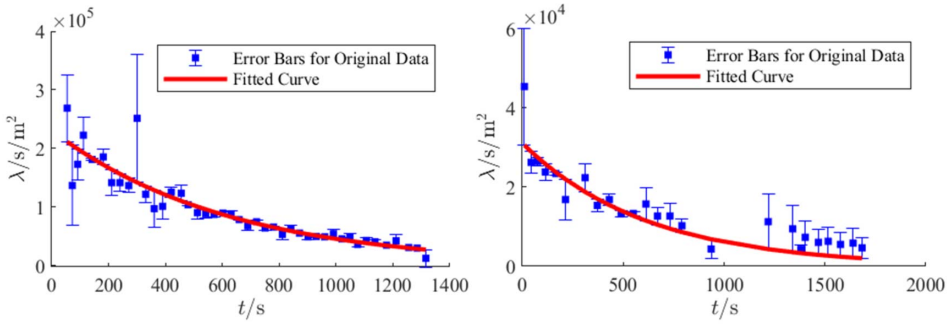

Figure 26: (a) nucleation rate for resin at room temperature (20°C), (b) nucleation rate for resin at 40°C.

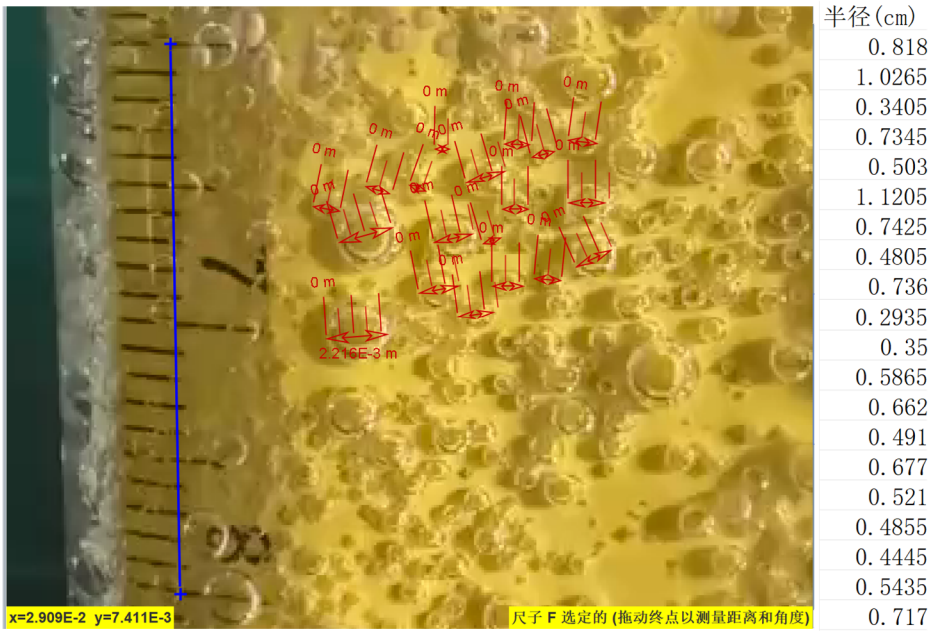

Figure 27: Measuring mean bubble size using an immersed ruler.

A.4. Determination of bubble size

To determine the size of the bubbles, and considering the curvature of the beaker wall and the magnification effect of water, we chose to use the scale on

a ruler as a calibration reference. By measuring the radii of different bubbles on the ruler, we obtained an average bubble radius. Using this average radius, we can then calculate the average volume of a single bubble.

The average radius is calculated to be $R_b = 6 \times 10^{-3}$m, and the average volume of the bubbles is $\overline{V} = 4\pi R_b^3/3 = 9 \times 10^{-7}\mathrm{m}^3$

A.5. Solving for pure rotational motion in Matlab (using ode45)

```
clc;
clear;
close all;
% Define constants
b=3;
Mc = 0.001; % Mass of chocolate, KG
Rc = 0.005; % Radius of a piece of chocolate
Rb = 0.0006;
theta0 = 45; % Angle at which the first bubble bursts
thetab = 0.06; % Angle occupied by a bubble
Sb = Rb^2; % Area occupied by a bubble
Ic = (2/5) * Mc * Rc^2; % Moment of inertia of chocolate
s = 1; % Assume a constant s
n = 4; % Width of the bubble band
rouC = 1.2; % Concentration of chocolate
rouw = 1; % Density of water
S0 = 1.666;
Smc = 0.002;
Tr = 2172; % 36.2min= this many seconds
chi = 2.5;
lambda0 = 58.4;
Vb = 4*pi*Rb^3/3;
g = 9.81;
Fb = Vb * g; % Force of a bubble, N
Tb1 = -Fb *1000* cosd(theta0) * Rc; % Torque of the first
bubble

% Package parameters into a structure
params.Tb1 = Tb1;
params.Ic = Ic;
params.Fb = Fb;
params.thetab = thetab;
```

```
params.Sb = Sb;
params.s = s;
params.theta0 = theta0;
params.n = n;
params.Rc = Rc;
params.rouC = rouC;
params.rouw = rouw;
params.g = g;
params.b = b;

% Calculate Nthresh and add it to the params structure
params.Nthresh = 84;
% Define time range and initial conditions
tspan = 0:0.01:10;
Theta0 = [0; 0; 0; 0; 0; 0; 0; 0]; % Initial conditions:
Theta(1) to Theta(6) are all initialized to 0
% 1. Theta break brought by Nbreak
% 2. Angular velocity brought by Nbreak
% 3. Thetanew brought by Nnew
% 4. Angular velocity brought by Nnew
% 5. Total angular displacement
% 6. Total angular velocity

Rt = @(t) 2.309E5 * exp(-0.001617 * t);
Rt_int = cumtrapz(tspan, Rt(tspan)); % Calculate the integral
of Rt from 0 to t

% Set absolute and relative solution accuracy
options = odeset('RelTol', 1e-9, 'AbsTol', 1e-12, 'Events',
@(t, Theta) events(t, Theta, params));

% Solve the differential equation using ode45
[t, Theta] = ode45(@(t, Theta) f(t, Theta, params, Rt_int,
tspan), tspan, Theta0, options);

% Ensure t and Rt_int are the same size
Rt_interp = interp1(tspan, Rt_int, t);
Nnet = (Theta(:, 5) / thetab .* (1 - Rt_interp .* Sb /
thetab ./ (1 + Rt_interp .* Sb)));
```

```
% Check calculation results
% disp('t:');
% disp(t);
% disp('Theta:');
% disp(Theta);
% disp('Rt_interp:');
% disp(Rt_interp);
% disp('Nnet:');
% disp(Nnet);
cosd(90)

% Plotting
figure;
plot(t, Nnet, 'LineWidth', 2, 'DisplayName', 'omega');
xlabel('$t$/s','interpreter','latex')
ylabel('$N broken$','interpreter','latex')
set(gca, 'FontSize',9,'FontName','Times New Roman')
set(gcf,'unit','centimeters','position',[10,10,8.5,8.5/1.618])

function dThdt = f(t, Theta, params, Rt_int, tspan)
    Tb1 = params.Tb1;
    Ic = params.Ic;
    Fb = params.Fb;
    thetab = params.thetab;
    Sb = params.Sb;
    s = params.s;
    theta0 = params.theta0;
    n = params.n;
    Rc = params.Rc;
    rouC = params.rouC;
    rouw = params.rouw;

    % Interpolate to calculate Rt_int
    R_integral = interp1(tspan, Rt_int, t, 'linear', 'extrap');

    dThdt = zeros(7, 1);
    dThdt(1) = Theta(2);
    dThdt(2) = Tb1 * n / Ic + Fb * n / Ic * (sind((Theta(5) +
thetab) / 2) * sind(Theta(5) / 2) / sind(thetab / 2));
    dThdt(3) = Theta(4);
```

```
    if dThdt(1)== 0
        dThdt(4)=0;
    else
    dThdt(4) = Fb / Ic * n * (-cosd(-thetab / 2 * (R_integral *
(Sb * (Theta(1) / Ic) / (1 + R_integral * Sb)))) - thetab +
Theta(5)) / ...
(2 * sind(-thetab / s));
    end
    dThdt(5) = Theta(6);
    %theta5 is the total rotation angle, instantaneous quantity
    %theta6 is the rotation speed, instantaneous quantity
    dThdt(7) = Theta(5) / thetab * (1 - R_integral * Sb /
thetab ./ (1 + R_integral * Sb));
    %is the net broken quantity, instantaneous quantity

    if Theta(7) < 0
        dThdt(6) = 0;
    else
        dThdt(6) = dThdt(2) + dThdt(4);
    end
end

function [value, isterminal, direction] = events(~, Theta,
params)
    b = params.b;
    Nthresh = params.Nthresh;
    % Define event function
    Ntot = Theta(7);
    if Ntot>=84
        b=0;
    end
    value = [b, Ntot];% When Ntot reaches Nthresh or is less
    than 0, trigger the event
    isterminal = [1,1]; % Stop integration
    direction = [0,-1]; % Trigger direction is any direction
end
```

A.6. Solving coupled motion ODE in MATLAB (using ode15s)

```
clc;
clear;
close all;

% Define constants
Mc = 0.001; % Mass of chocolate, KG
Rc = 0.005; % Radius of a piece of chocolate
Rb = 0.0005;
theta0 = 0.1; % Angle at which the first bubble bursts
thetab = 0.06; % Angle occupied by a bubble
Sb = Rb^2; % Area occupied by a bubble
Ic = (2/5) * Mc * Rc^2; % Moment of inertia of chocolate
s = 1; % Assume a constant s
n = 4; % Width of the bubble band
rouc = 1.2; % Concentration of chocolate
rouw = 1; % Density of water
% S0 = 1.66;
% Smc = 0.002;
Tr = 2172; % 36.2 minutes = this many seconds
% chi = 2.5;
% lambda0 = 58.4;
Vb = 4*pi*Rb^3/3;
g = 9.81;
Fb = Vb * g*1000; % Force of a bubble, N
Tb1 = -Fb * cosd(theta0) * Rc*5; % Torque of the first bubble
(approximate size of perturbation)
phi = rouw / rouc;
eta = 1.1E-3; % Viscosity coefficient
max = 4*pi*Rc^2/Sb;
% Package parameters into a structure
params.Tb1 = Tb1;
params.Ic = Ic;
params.Fb = Fb;
params.thetab = thetab;
params.Sb = Sb;
params.s = s;
params.theta0 = theta0;
params.n = n;
```

```
params.Rc = Rc;
params.rouc = rouc;
params.rouw = rouw;
params.g = g;
params.phi = phi;
params.eta = eta;
params.Vb = Vb;
params.Nthresh = 84;
params.max = max;

% Define initial conditions
tspan = 0:0.01:30; % Initial time range
Theta0 = [0; 0; 0; 0; 0; -0.01; 0; -0.09; 0; 0; 0];
% 1. Theta break brought by Nbreak
% 2. Angular velocity brought by Nbreak
% 3. Thetanew brought by Nnew
% 4. Angular velocity brought by Nnew
% 5. Total angular displacement
% 6. Total angular velocity
% 7. Total amount of broken bubbles
% 11. integral of Theta7
% 8. Vertical acceleration
% 9. Vertical velocity
% 10. Vertical displacement

% Define Rt function
Rt = @(t) 2.309E5 * exp(-0.001617 * t);
Rt_integral = cumtrapz(tspan, Rt(tspan)); % Calculate the
integral of Rt from 0 to t

% Initialize Theta and Nnet variables
% Theta = Theta0;
% Nnet = [];

% Check if there is enough data for plotting
% Set absolute and relative solution accuracy
options = odeset('RelTol', 1e-9, 'AbsTol', 1e-12);
% Solve the differential equation using ode45
[t, Theta] = ode15s(@(t, Theta) f(t, Theta, params), tspan,
Theta0, options);
```

```
%%
% Check if the integral of Theta(:,7) is less than 0
Theta7 = Theta(:,7);
D = zeros(size(Theta7)); % Initialize D according to the size
of Theta7
for i = 1:(length(Theta7)-1)
    D(i+1) = D(i) + Theta7(i);
end
position = find(D < 0, 1);

% Do not check
% position = length(tspan);
%%

% Plotting
figure;
% subplot(3, 1, 1);
% plot(tspan(1:position), Theta(1:position,11), 'LineWidth', 1,
'DisplayName', 'Nnet');
% xlabel('$t$/s','interpreter','latex')
% ylabel('$Nnet /\rm{s^-1}$','interpreter',
'latex')
% set(gca, 'FontSize',9,'FontName','Times New Roman')
% %set(gcf,'unit','centimeters','position',[10,10,8.5,
8.5/1.618])
% hold on;
%
% subplot(3, 1, 2);
% plot(tspan(1:position), Theta(1:position, 8), 'LineWidth', 1,
'DisplayName', 'y'); %8
% xlabel('$t$/s','interpreter','latex')
% ylabel('$y$/m','interpreter','latex')
% set(gca, 'FontSize',9,'FontName','Times New Roman')
% %set(gcf,'unit','centimeters','position',[10,10,8.5,
8.5/1.618])
% hold on;

plot(tspan(1:500), Theta(1:500, 6)*pi/180, 'LineWidth', 1.5,
'Color',[1,0.75,0.5]); %6
xlabel('$t$/s','interpreter','latex')
```

```
ylabel('$\omega$ rad/s','interpreter','latex')
set(gca, 'FontSize',9,'FontName','Times New Roman')
set(gcf,'unit','centimeters','position',[10,10,8.5,8.5/1.618])
hold on;
%%

% % Event function: Detect when y(1) reaches -0.09
% function [value, isterminal, direction] =
event_y_reaches_threshold(~, y)
% value = y(1) + 0.09; % Event condition
% isterminal = 1; % Stop when the event occurs
% direction = 0; % Detect the direction of decrease, 0 means
either side is okay
% end

% Differential equations for Theta
function dThdt = f(t, Theta, params)
Tb1 = params.Tb1;
Ic = params.Ic;
Fb = params.Fb;
thetab = params.thetab;
Sb = params.Sb;
Rc = params.Rc;
n = params.n;
s = params.s; % Use the s variable passed in params.s
Vb = params. Vb;

%% Convert Rt_integral1 to a function of t
% Method 1
% tspan = 0:0.01:t;
% Rt = @(a) 2.309E5 * exp(-0.001617 * a);
% Rt_integral1 = max(cumtrapz(tspan, Rt(tspan)));
% Method 2
Rt_integral1 = (-(2.309E5/0.001617)*exp(-0.001617 *
t))-(-(2.309E5/0.001617)*exp(-0.001617 * (0)));

%%
dThdt = zeros(11, 1); % Initialize

% Theta3 corresponds to the angular displacement brought by
```

```
Nnew, Theta4 is the angular velocity. Bubbles will continue to
generate whether below the liquid surface or not, so no
conditional judgment is needed

dThdt(3) = Theta(4);
dThdt(4) = Rt_integral1*(4*pi*Rc^2)*Vb*1000;

% Theta1 corresponds to the angular displacement brought by
Nbreak, Theta2 corresponds to its angular velocity
% If the submerged object is already at the liquid top (-0.09m,
taking downward as positive), then calculate it with the
rotation formula, otherwise set it to 0, because at this point
rotation will not lead to bubble rupture
dThdt(1) = Theta(2);
if Theta(8) < -0.09
dThdt(1) = 0;
dThdt(4) = Fb*Rc / Ic * n * (-cosd(-thetab / 2 *
(Rt_integral1 .* (Sb * (Theta(1) ./ Ic) ./ (1 + Rt_integral1 *
Sb)))) - thetab + Theta(5)) ./ ...
(2 * sind(-thetab ./ s));
dThdt(7)=(dThdt(2)-dThdt(4))/thetab;
else
dThdt(7) = -Rt_integral1*(4*pi*Rc^2)*Vb*1000;
dThdt(2) = Tb1 .* n ./ Ic + Fb .* n *Rc./ Ic *
(sind((Theta(5) + thetab) ./ 2) * sind(Theta(5) ./ 2) ./
sind(thetab ./ 2));
end
% Theta5 corresponds to the total angular displacement,
Theta6 corresponds to the net angular velocity, Theta7 is the
total amount of broken bubbles

dThdt(10) = Theta(5);
dThdt(5) = Theta(6);
if Theta(8) <= -0.09
dThdt(7) = Theta(5) ./ thetab * (1 - Rt_integral1 * Sb ./
thetab ./ (1 + Rt_integral1 * Sb));
else
dThdt(7) = 0;
end
max = params.max;
```

```
Rt = 2.309E5 * exp(-0.001617 * t);
% If the total amount of broken bubbles is less than or equal
to 0, it means the bubbles have covered the surface, then new
bubbles will not be generated, and the angular acceleration
brought by Nnew dThdt(4) will also be 0
% On the contrary, the net angular acceleration is equal to the
sum of the breaking and generating accelerations
dThdt(11) = Theta(7);
if Theta(11) <= 0
dThdt(3) = 0; % The bubbles have covered the surface
dThdt(7) = -dThdt(2)/thetab*Sb*Rt;
elseif Theta(11) <= 200
dThdt(6) = -dThdt(2) - dThdt(4);
else
dThdt(5) = 0;
end

phi = params.phi;
Rc = params.Rc;
eta = params.eta;
g = params.g;
Vb = params.Vb;
rouc = params.rouc;

% Calculate Rt_integral directly using t
% Rt_integral = integral(@(t_var) Rt(t_var), 0, t);
%Initialization
%Theta81 is the vertical displacement, positive downward
%Theta92 is the vertical velocity, positive downward
dThdt(8) = Theta(9);

% If the submerged object is already at the liquid surface, and
the total amount of broken bubbles is less than the Threshold
(more than this amount the buoyancy provided by the bubbles
will not be able to support the object from floating), then y
remains unchanged
% On the contrary, use the formula mentioned in the text to
calculate
% If it is not at the liquid surface (starting from line 213),
if the submerged object is at the bottom and the total amount
```

```
of broken bubbles is greater than the threshold, then the
vertical acceleration is 0
% On the contrary, calculate according to the formula
(1 - phi) * Rc / (3 * phi * Vb)
if Theta(8) <= -0.09 && Theta(7) < 200
dThdt(8) = 0;
elseif Theta(8) >=0 && Theta(7)/thetab > 200
dThdt(8) = 0;
dThdt(11) = 0;
else
dThdt(9) = (1 - phi) * g - (5 * eta / (2 * Rc^2 * rouc) *
Theta(9)) - (2 * phi * Rt_integral1 * Vb* g) / Rc;
end
end
```

Acknowledgments

Over the past six months since the inception of our research, every team member has dedicated passion and effort, culminating in the opportunity to present our project in the final round of the Yau High School Science Award. The division of labor for this research is as follows: Haiyi Luo carried out the theoretical derivation of the nucleation rate and the translational-rotational dynamics of small spheres in carbonated water, wrote all numerical simulation programs, and proposed a new method for determining bubble nucleation rates. She also designed and created submerged objects of various shapes and materials to assist in qualitative and quantitative experiments on nucleation rate determination, translational and rotational rate measurements, and the combined frequency analysis of translation and rotation. Additionally, she authored the first and second sections of the paper. Yunyi Yang contributed by proposing an explanation and calculation method for the experimental phenomena observed in the initial phase of the research. He processed and plotted all experimental data, conducted quantitative experiments using small spheres made of chocolate, resins, and other materials, and participated in revising the paper during its later stages.

As this paper concludes, we sincerely thank those who supported us throughout this journey. First, we extend our heartfelt gratitude to our mentor, Mr. Zhang Chengxin. When we first observed the irregular motion of chocolate in carbonated water, Mr. Zhang encouraged our exploration of this novel phenomenon. His profound theoretical knowledge and practical expertise greatly enriched our research experience. From advising us to place a

ruler in the beaker to mitigate distortion effects caused by the carbonated water and container, to recommending different materials to better validate our theory, Mr. Zhang tirelessly guided us with systematic research methods, providing a strong foundation for our future studies.

Lastly, we are deeply grateful to our parents for their unwavering support. Their financial assistance enabled us to purchase small spheres of various sizes and materials, allowing us to collect multiple sets of experimental data. Their encouragement and backing were essential to the successful completion of this research and the writing of this paper. In conclusion, we also thank all the teachers and students of Chongqing Yucai Middle School for their care and encouragement. It was everyone's support that allowed us to persevere and complete this research to a high standard.

References

[1] S. Lubetkin and M. Blackwell The nucleation of bubbles in supersaturated solutions. *J. Colloid Inter. Sci.* **126**, 610 (1988).

[2] L. E. Scriven On the dynamics of phase growth. *Chem. Eng. Sci.* **10**, 1 (1959).

[3] R. P. Sear Nucleation: theory and applications to protein solutions and colloidalsuspensions. *J. Phys.: Condens. Matter.* **19**, 3 (2007).

[4] Á. M. Soto, T. Maddalena, A. Fraters, D. Van Der Meer and D. Lohse Coalescence of diffusively growing gas bubbles. *J. Fluid Mech.* **846**, 143 (2018). MR3797921

[5] S. E. Spagnolie, S. Christianson and C. Grote Levitation and dynamics of bodies in supersaturated fluids. *Nat. Commun.* **15**, 3910 (2024).

[6] R. S. J. Sparks The dynamics of bubble formation and growth in magmas: a review and analysis. *J. Volcanol. Geotherm. Res.* **3**, 1 (1978).

[7] A-Man Zhang, Shi-Min Li, Pu Cui, Shuaitong Li and Yunlong Liu. A unified theory for bubble dynamics. *Physics of Fluids* **35**, 033323 (2023).

Haiyi Luo
Chongqing Yucai Secondary School
China
E-mail address: lhyiris@outlook.com

Yunyi Yang
Chongqing Yucai Secondary School
China
E-mail address: 932525090@qq.com